CrossMark

Injectable nanomedicine hydrogel for local chemotherapy of glioblastoma after surgical resection

C. Bastiancich[a,c,d], J. Bianco[a], K. Vanvarenberg[a], B. Ucakar[a], N. Joudiou[b], B. Gallez[b], G. Bastiat[c,d], F. Lagarce[c,d], V. Préat[a,*], F. Danhier[a]

[a] Université catholique de Louvain, Louvain Drug Research Institute, Advanced Drug Delivery and Biomaterials, Brussels, Belgium
[b] Biomedical Magnetic Resonance Research Group, Louvain Drug Research Institute, Université Catholique de Louvain, Brussels, Belgium
[c] MINT, UNIV ANGERS, INSERM 1066, CNRS 6021, Université Bretagne Loire, Angers, France
[d] Pharmacy Department, UFR Santé, Université Bretagne Loire, Angers, France

ARTICLE INFO

ABSTRACT

Glioblastoma (GBM) treatment includes, when possible, surgical resection of the tumor followed by radiotherapy and oral chemotherapy with temozolomide, however recurrences quickly develop around the resection cavity borders leading to patient death. We hypothesize that the local delivery of Lauroyl-gemcitabine lipid nanocapsule based hydrogel (GemC$_{12}$-LNC) in the tumor resection cavity of GBM is a promising strategy as it would allow to bypass the blood brain barrier, thus reaching high local concentrations of the drug. The cytotoxicity and internalization pathways of GemC$_{12}$-LNC were studied on different GBM cell lines (U251, T98-G, 9L-LacZ, U-87 MG). The GemC$_{12}$-LNC hydrogel was well tolerated when injected in mouse brain. In an orthotopic xenograft model, after intratumoral administration, GemC$_{12}$-LNC significantly increased mice survival compared to the controls. Moreover, its ability to delay tumor recurrences was demonstrated after perisurgical administration in the GBM resection cavity. In conclusion, we demonstrate that GemC$_{12}$-LNC hydrogel could be considered as a promising tool for the post-resection management of GBM, prior to the standard of care chemo-radiation.

1. Introduction

Glioblastoma (GBM) is the most aggressive and lethal brain tumor in adults. It is a grade IV astrocytoma characterized by rapid proliferation, high infiltration capacity, chemoresistance and ability to quickly form recurrences, even after multiple surgery and treatment [1]. GBM can be divided into IDH-wildtype GBM (90%) which arises in an acute *de novo* manner without previous lower grade pathology or symptoms, or into IDH-mutant GBM (10%) which derives from the progressive evolution and transformation of lower grade astrocytomas and normally affects younger patients [2]. In both cases, maximal safe surgical resection of the accessible primary tumor is the first and most important step in the management of these tumors, but it can only be applied to 65–75% of GBM patients [3,4]. Following resection, GBM patients are generally treated with standard treatment regimens which include radiotherapy plus concomitant and adjuvant oral chemotherapy with the alkylating agent Temozolomide (TMZ) [5]. However, recurrences develop at the resection border margins (90% of cases) or in other regions of the brain within two years leading, in most of the cases, to death [6,7]. Indeed,

despite the efforts of the scientific community, the prognosis for GBM patients remains poor (median survival < 15 months), 2- and 4- year survival rates are 27% and 10% respectively and the long-term survivors are nearly inexistent [8,9].

Limitations in the effectiveness of current standard of care treatments are amplified through the formation of GBM recurrences due to several hurdles. The anatomical location of the tumor interferes with a complete surgical resection while the presence of the blood-brain barrier (BBB) limits the number of cytotoxic drugs that can effectively reach the tumor site at therapeutic concentrations. In addition, GBM cells widely diffuse into the brain parenchyma, and their tendrils are often undetectable by imaging techniques. Moreover, cancer stem cells with high tumorigenic ability, self-renewal potential and strong resistance to radio and chemotherapy have been recognized in gliomas [10–13]. As chemoradiation can have an impact on the wound healing process, GBM patients generally follow the standard radio- and chemotherapy regimen several weeks after surgery, once the wound has healed [14]. During this time gap, the residual tumor cells can proliferate around the resection cavity borders. Further difficulties in

treatment are brought about by the high heterogeneity of GBM cells combined to their innate and acquired chemoresistance, reducing the efficacy of TMZ. Indeed, only one third of GBM patients are responsive to alkylating agents [13,15,16].

In the last decades, many strategies have been adopted to increase the therapeutic efficacy and survival rate of GBM patients (*e.g.* gene therapy, immunotherapy, targeted therapy, nanomedicines, ultrasounds, etc.) [17–22]. Among them, the local delivery of chemotherapeutic drugs in the tumor resection cavity has shown a promising role [23–25]. This approach aims at increasing the local concentrations of the drugs, subsiding systemic side effects, while also reducing the lapse of time between resection and the chemotherapy which in turn prevents the growth of the remaining cancer cells, often responsible of recurrences. Gliadel®, a carmustine-loaded biodegradable wafer, is the most-successful and the only local delivery implant currently approved by the FDA for GBM [26,27]. Its use has shown modest effect in prolonging the overall survival of GBM patients but tumor recurrences have been reported in the majority of treated cases. To improve the sustained intracerebral drug release and overcome limitations such as local side effects, poor drug penetration depth and implant dislodgements, many researchers are currently focusing on the local delivery of cytotoxic drugs through different delivery systems (*e.g.* foams, films, membranes, hydrogels) [25,28]. Our group is mainly focused on craniotomy-based drug delivery *via* anti-cancer loaded hydrogels [29,30]. These injectable and adaptable systems can be implanted or injected into the resection cavity immediately after surgery and can guarantee a sustained release of the drug in the surrounding brain tissue over time. Some hydrogels are also administrable intratumorally in non-operable GBM tumors [31]. Several aspects need to be considered when developing an effective anticancer drug loaded hydrogel for the local treatment of GBM. Firstly, choosing a drug that does not interfere with the mechanisms of action or the chemoresistance pathways of TMZ, and could have radiosensitizing and/or synergic properties with the standard treatments is of importance. Secondly, the release profile of the drug from the hydrogel should be controlled and sustained over time. Finally, the system should be injectable, degradable and well tolerated. It should have mechanical properties compatible with the brain tissue and possibly adapt to the resection cavity and adhere to the brain parenchyma [25].

Recently, we proposed the use of an innovative hydrogel uniquely formed of lipid nanocapsules (LNC) and Lauroyl-gemcitabine (GemC$_{12}$) for the local treatment of GBM [29]. This injectable nanomedicine hydrogel presents mechanical properties adapted for brain implantation and allows a sustained release of the drug over 1 month *in vitro*. *In vivo*, this system is well tolerated during one week in mouse brain and reduces tumor growth in a subcutaneous human GBM model, when compared to free drug.

In this paper, we hypothesize that GemC$_{12}$-LNC nanomedicine hydrogel could improve the GBM recurrences management when injected in the tumor resection cavity immediately after surgery. Therefore, (i) the *in vitro* cytotoxicity and cellular uptake, (ii) the *in vivo* mid- and long-term tolerability in mouse brain, and (iii) the antitumor efficacy of the hydrogel after intratumoral injection in an orthotopic human xenograft GBM model and after local administration in the resection cavity in an orthotopic resection model were investigated.

2. Materials and methods

2.1. Formulation of GemC$_{12}$ lipid nanocapsules hydrogel (GemC$_{12}$-LNC)

The gel formulation GemC$_{12}$-LNC was prepared using a phase-inversion method previously reported in the literature [32]. Briefly, 0.093 g of GemC$_{12}$ (synthesized as previously described [33]), 1.24 g of Labrafac® (Gattefosse, France) and 0.25 g of Span 80 (Sigma-Aldrich, USA) were weighed and stirred in a water bath at 50 °C with 200 μL of acetone (VWR Chemicals, Belgium) until complete dissolution of the

drug. The acetone was then allowed to evaporate and 0.967 g of Kolliphor® (Sigma-Aldrich, Germany), 0.045 g of Sodium Chloride (VWR Chemicals, Belgium) and 1.02 g of injectable water (Braun, Germany) were added to the formulation. Three cycles of heating and cooling were performed under magnetic stirring (500 rpm) between 40 and 70 °C. During the last cooling cycle, at the temperature corresponding to the phase-inversion zone, 2.12 g of injectable water was added and the formulation stirred for one more minute. The formulations were then inserted into insulin syringes (BD Micro-Fine™ needle 0.30 mL, Ø 30 G; Becton Dickinson, France) before the gelation process occurred, and stored at 4 °C until further use. The unloaded LNC were obtained using the same method without adding the active compound. For the fluorescent-labeled LNC, 83.4 μL of the fluorescent DiD fluorophor (1,1′-Dioctadecyl-3,3,3′,3′-Tetramethylindodicarbocyanine 4-Chlorobenzenesulfonate salt, Thermo Fischer Scientific, USA; 1 mg/mL solution in absolute ethanol), were added to the first step of the formulation process, which was then carried on as previously described protected from the light. All the formulations were obtained under aseptic conditions.

2.2. In vitro cellular studies

2.2.1. Cell cultures

U251, T98-G and U-87 MG glioma cells (ATTC, USA) were cultured in Eagle's Minimum Essential Medium (EMEM; ATTC, USA) while 9L-LacZ cells (ATTC, USA) were cultured in Dulbecco's modified Eagle's Medium with 4.5 g/L glucose, 0.58 g/L L-glutamine and 0.11 g/L sodium pyruvate (DMEM; Gibco, Life Technologies, USA). Medias were supplemented with 10% Fetal Bovine Serum (FBS; Gibco, Life Technologies USA), 100 U/mL penicillin G sodium and 100 μg/mL streptomycin sulfate (Gibco, Life Technologies, USA). Cells were subcultured in 75 cm^2 culture flasks (Corning® T-75, Sigma-Aldrich, USA) and incubated at 37 °C and 5% CO$_2$.

2.2.2. Cytotoxicity studies (crystal violet assay)

Cytotoxicity assays were performed using crystal violet staining after 48 h of incubation with different concentrations of GemHCl, GemC$_{12}$ or GemC$_{12}$-LNC with or without the hENT1 transporter inhibitor dypiridamole (Dyp; Sigma Aldrich, USA). Cells were seeded at a density of 2.5–5 × 10^3 cells/well depending on the cell type in 96-wells plates and incubated at 37 °C and 5% CO$_2$. To obtain a cell monolayer and obtain homogenous adhesion of the cells throughout the wells, for U-87 MG cell line wells were previously coated with poly(D)lysine (PDL; 0.1 mg/mL per well; Sigma-Aldrich, USA) and then rinsed with phosphate buffered saline (PBS; Gibco, Life Technologies USA) before being plated and incubated at 37 °C and 5% CO$_2$[29]. They were then either incubated with Triton X-100 (Sigma-Aldrich, USA), different concentrations of Gemcitabine Hydrochloride (GemHCl; Sigma-Aldrich, USA), GemC$_{12}$, GemC$_{12}$-LNC, unloaded LNC or left untreated. The treatments were dissolved in PBS (GemHCl, GemC$_{12}$-LNC and unloaded LNC) or in Water/Ethanol/Tween® 80 6.9/87.6/5.5 v/v (GemC$_{12}$; [34]) and then suitably diluted in complete culture medium. The concentration of active drug ranged between 0.01 and 25 μM. To study the effect of nucleoside transport inhibitors on drug sensitivity, cells were exposed to Dyp (10 μM) before and during the treatments incubation to inhibit hENT1 transporters [35]. After 48 h of incubation with the treatments, cells were fixed with 10% formalin solution (Merck, Germany) for 20 min and then stained with Crystal violet solution (0.5% in 20% Methanol) for 20 min. The plates were then rinsed with distilled water multiple times, air-dried and observed at the microscope. Methanol was added to the wells and spectrophotometric readings were performed after 30 min at 560 nm with a MultiSkan EX plate reader (Thermo Fisher Scientific, USA). Cells cultured with complete culture medium or Triton X-100 were considered as negative and positive controls, respectively. Results are expressed as relative percentage of living cells compared to the negative control (untreated cells) (N = 3,

$n = 18$).

2.2.3. Cellular uptake and internalization studies

Cellular uptake of fluorescent-labeled (DiD) unloaded LNC or GemC$_{12}$-LNC (0.06 mg·g^{-1} DiD/Labrafac) was quantified by flow cytometry. Glioma cell lines were seeded in 12-well plates (8×10^4 cells/well for 9L-LacZ cells; 1.2×10^5 cells/well for U251, T98G and U-87 MG cells) and incubated at 37 °C, 5% CO$_2$ overnight. Cells were then incubated at 4 °C or 37 °C with Hanks' Balanced Salt Solution (HBSS, control; Gibco, Life Technologies USA), unloaded DiD-LNC or DiD-GemC$_{12}$-LNC (1.21 mg/mL LNC in HBSS) for 1 h or 8 h. At the end of the incubation time, cells were rinsed with PBS, trypsinized and diluted with medium. After centrifugation ($250 \times g$, 5 min, 4 °C), the cell pellet was resuspended in 300 μL PBS. Measurements were performed using a FACSscan cytometer (FlowJo software). The procedure was repeated in three independent experiments, and at least 2000 cells were analyzed in each measurement.

Cellular internalization was also observed by fluorescent microscopy. For this experiments, 12 well-plates containing one PDL-coated coverslip (as previously described) per well were used. Cells were seeded in the wells (8×10^4 cells/well for 9L-LacZ cells; 1.2×10^5 cells/well for U251, T98G and U-87 MG cells) overnight before being incubated at 4 °C or 37 °C with unloaded DiD-LNC or DiD-GemC$_{12}$-LNC for 1 h or 8 h. At the end of the incubation time, cells were fixed with 2% paraformaldehyde (5 min, room temperature), rinsed three times with PBS and incubated for 1 h at room temperature with Concanavalin A Alexa Fluor® 488 conjugate (ConA) in the dark. Cells were then rinsed three times and coverslips were mounted on slides using Vectashield HardSet mounting medium (with DAPI; Labconsult, Belgium) and stored at −20 °C until further use. Slides were examined under an inverted fluorescent microscope (Apotome, Zeiss, Belgium) with 350 nm (blue, DAPI; cell nuclei), 488 nm (green, ConA; cell membranes) and 647 nm (red, DiD; LNC) excitation filters.

2.3. In vivo studies

All experiments were performed following the Belgian national regulations guidelines as well as in accordance with EU Directive 2010/63/EU, and were approved by the ethical committee for animal care of the faculty of medicine of the Université catholique de Louvain (2014/UCL/MD/004). Animals had free access to water and food. Animal body weight was constantly monitored throughout the experiments.

2.3.1. Mid- and long-term tolerability assays

Seven-week-old female NMRI mice (Janvier, France) were randomly divided into 4 groups. On day one, mice were anesthetized by intraperitoneal injection of ketamine/xylazine (66.6 and 8.6 mg/kg, respectively) and a hole was created in the skull at the left frontal lobe using a high-speed drill (Dremel Inc., USA). Ten μL of either sterile PBS solution, unloaded LNC or GemC$_{12}$-LNC hydrogel was injected in the hole. This volume corresponds to the maximal amount allowed for intracerebral injection in mice. A fourth group included animals administered with 2.5 μL of GemC$_{12}$ (the injected volume was reduced for this group as the drug is dissolved in Water/Ethanol/Tween®80 6.9/87.6/5.5 v/v/v). The amount of drug administered in the drug treated groups corresponded to 5.5 mg/kg of GemC$_{12}$. Mice were then sutured and observed for two or six months (mid- or long-term, respectively). After this time, mice were sacrificed and brains were removed and fixed in 10% formalin solution (Merck, Germany) for 20 h before being rinsed in PBS and kept at 4 °C for at least two days. Brains were then embedded in paraffin, sectioned at 10 μm using a MICROM 17M325 microtome (Thermo Fischer Scientific, USA) and collected on superfrost plus glass slides. Slides were incubated at 37 °C overnight before being stored at room temperature until further use.

For the histological analysis and evaluation of the cellular inflammatory response the samples were deparaffinized and stained with hematoxylin and eosin (H & E) ($n = 5$ for mid-term experiments, $n = 3$ for long-term experiments) using a Sakura DRS 601 automated slide stainer (Sakura Finetek Europe, The Netherlands).

For the TUNEL assay, the Dual End Fluorometric TUNEL System kit ® (Promega, USA) was used following manufacturer instructions. Slides were mounted with Vectashield HardSet mounting medium (with DAPI; Vector Laboratories, USA) and examined under an inverted fluorescent microscope (Apotome, Zeiss, Belgium) with 350 nm (blue, DAPI) and 748–789 nm (green, TUNEL) excitation filters ($n = 5$ for mid-term experiments, $n = 3$ for long-term experiments).

Microglia activation was evaluated by Iba-1 immunostaining. Slides were deparaffinized, endogenous peroxidases were blocked with hydrogen peroxide (30% v/v) and then left for 90 min in citrate buffer in a water bath at 100 °C. Sections were then incubated for 30 min with 10% normal horse serum to block non-specific binding sites before incubation with a goat anti-human Iba-1 antibody (1:1000; Novus Biologicals, USA) overnight at room temperature. Slides were then rinsed and incubated for 60 min at room temperature with rabbit anti-goat IgG biotinylated antibody (1:200; Vector Laboratories, USA). Sections were then counterstained with hematoxylin, dehydrated and mounted with DPX neutral mounting medium (Prosan, Belgium). Slides were scanned using a SCN400 Leica slide scanner and image analysis was performed with Digital Image Hub (Leica, Germany) ($n = 5$ for mid-term experiments, $n = 3$ for long-term experiments).

2.3.2. Orthotopic U-87 MG human glioblastoma tumor model

Six-week-old female NMRI nude mice (Janvier, France) were anesthetized by intraperitoneal injection of ketamine/xylazine (100 and 13 mg/kg, respectively), fixed in a stereotactic frame and 3×10^4 U-87 MG glioma cells were injected in the right frontal lobe using a Hamilton syringe as previously described [36,37]. The injection coordinates for the orthotopic model and resection model were 0.5 mm anterior or posterior, 2.1 mm lateral from the bregma and 2.5–3 mm deep from the outer border of the cranium, respectively. The presence, volume and location of the tumors were determined by Magnetic Resonance Imaging (MRI), which was performed for all mice included in the study between day 9 and 13 post tumor cell implantations.

2.3.3. MRI

MRI was performed using a 11.7 T Bruker Biospec MRI system (Bruker, Germany) equipped with a ^{1}H quadrature transmit/receive surface cryoprobe after anesthetising animals with isoflurane mixed with air (2.5% for induction, 1% for maintenance). Respiration was continuously monitored while animal core temperature was maintained throughout the experiment by hot water circulation in the cradle. Tumor volume was assessed using rapid acquisition with relaxation enhancement (RARE) sequence (TR = 2500 ms; effective echo time (TE$_{eff}$) = 30 ms; RARE factor = 8; FOV = 2×2 cm; matrix 256×256; twenty-five contiguous slices of 0.3 mm, NA = 4). Tumor volumes were calculated from a manually drawn region of interest (ROI).

2.3.4. Anti-tumor efficacy of GemC$_{12}$-LNC hydrogel after intratumoral administration in an orthotopic U-87 MG human glioblastoma tumor

At day 15 post-tumor inoculation mice were randomly divided into six groups and treated intratumorally, intravenously or left untreated. For the local treatment, mice were anesthetized, fixed in a stereotactic frame and treatments were injected in the previous burr hole using a 0.3 mL insulin syringe (GemC$_{12}$-LNC hydrogel and unloaded LNC) or a Hamilton syringe fitted with a 32G needle (GemHCl and GemC$_{12}$). For intravenous treatment, mice were injected through the tail vein. **Group 1:** control group (no treatment) ($n = 11$); **Group 2:** intratumoral injection of unloaded LNC, 5 μL ($n = 7$); **Group 3:** intratumoral injection of GemHCl, 2.5 μL ($n = 7$); **Group 4:** intratumoral injection of GemC$_{12}$ dissolved in Water/Ethanol/Tween®80 (6.9/87.6/5.5 v/v), 2.5 μL ($n = 7$); **Group 5:** intravenous injection of GemC$_{12}$ solubilised as

previously mentioned and diluted in sterile PBS, 100 μL ($n = 7$); **Group 6:** intratumoral injection of GemC$_{12}$-LNC gel, 5 μL ($n = 9$). The dose of drug injected was 3 mg/kg of GemC$_{12}$. The delivered dose of unloaded LNC was the same as GemC$_{12}$-LNC.

2.3.5. Anti-tumor efficacy of GemC$_{12}$-LNC hydrogel after peritumoral administration in the U-87 MG tumor resection cavity

At day 13 post-tumor inoculation, the tumor resection was performed using the biopsy-punch resection model, as previously described by Bianco et al. [37]. Briefly, animals were anesthetized with ketamine/xylazine and immobilised in a stereotactic frame. A 7 mm incision was made in the midline along the previous surgical scar and a 2.1 diameter circular cranial window was created around the previous burr hole to expose the brain using a high-speed drill (Dremel Inc., USA). A 2 mm Ø biopsy punch (Kai Medical, Germany) was then inserted 3 mm deep and twisted for 15 s to cut the brain/tumor tissue. Once withdrawn, the tumor and brain tissues were aspirated using a diaphragm vacuum pump (Vaccubrand GMBH + CO KG, Germany). Between 2.5 and 5 μL of treatment (depending on the group) was placed into the resection cavity before sealing the cranial window with a 4 mm × 4 mm square piece of Neuro-Patch® (Aesculap, Germany) impregnated with a re-constituted fibrin hydrogel (25 mg/mL fibrin, 10 IU/mL thrombin, equal volumes; Baxter Innovations, Austria). **Group 1:** control group (no treatment) ($n = 10$); **Group 2:** unloaded LNC, 5 μL ($n = 7$); **Group 3:** GemHCl, 2.5 μL ($n = 7$); **Group 4:** GemC$_{12}$ dissolved in Water/Ethanol/Tween®80 (6.9/87.6/5.5 v/v), 2.5 μL ($n = 7$); **Group 5:** GemC$_{12}$-LNC gel, 5 μL ($n = 7$). The dose of drug administered was 3 mg/kg of GemC$_{12}$. The delivered dose of unloaded LNC was the same as GemC$_{12}$-LNC. For both anti-tumor efficacy studies, mice were sacrificed when they presented ≥ 20% body weight loss or 10% body weight loss plus clinical signs of distress (paralysis, arched back, lack of movement).

2.4. Statistical analysis

Statistical analysis was performed using GraphPad Prism (GraphPad Software, USA) and determined based on $p < 0.05$. For the *in vitro* cytotoxicity studies, Kruskal-Wallis test + Dunn multiple comparison post-test was performed for Fig.1, while two-way ANOVA test with Bonferroni post-test were used for Fig. 2. In these experiments, N corresponds to the number of independent experiments performed while n is the number of replicates for each experiment. Results are expressed as mean ± standard deviation (SD) of at least three independent experiments. For the *in vivo* efficacy studies, the statistical analysis was estimated from comparison of Kaplan-Meier survival curves using the log-rank test (Mantel Cox test). Outliers were calculated using GraphPad software (significance level 0.01, two-sided) and removed from the study.

3. Results and discussion

3.1. In vitro cytotoxicity of GemC$_{12}$-LNC in GBM cell lines with or without nucleoside transporter inhibition

We previously demonstrated, using the MTT assay, a higher cytotoxicity of GemC$_{12}$ and GemC$_{12}$-LNC compared to the parent drug GemHCl on the U-87 MG cell line, hypothesizing that this result was due to differences in the internalization mechanisms of the drugs [29]. Gemcitabine is a nucleoside analogue and its cellular uptake requires the presence of specialized plasma membrane nucleoside transporters (NT), either sodium-independent (equilibrative nucleoside transporters hENT1 and hENT2) or sodium-dependent (concentrative nuclear transporters hCNT1, hCNT2 and hCNT3). The different distribution of these NT in cells and tissues as well as their different ability to transport nucleoside analogs is related to the different drug response (*e.g.* sensibility to the drug, chemoresistance) [35,38]. Gemcitabine is

preferentially directed by hENT1 and several studies have shown that higher levels of this transporter are associated to a better response to the drug [33,39]. Hence, to evaluate if there is a difference between the internalization pathways of GemHCl, the alkylated drug GemC$_{12}$ and GemC$_{12}$-LNC, we tested if their cytotoxic activity in four GBM cell lines is affected by the inhibition of the hENT1 transporter. We performed crystal violet staining after 48 h of incubation with different concentrations of the drugs, with or without incubation with dypiridamole (Dyp), which can specifically block the hENT1 transporter [35,40]. Dyp significantly inhibited GemHCl uptake in U251 (Fig. 1A) and T98G cells (Fig. 1B), as shown by a reduced cytotoxic effect of the drug at concentrations of 0.1, 1 and 10 μM compared to the cells without Dyp ($p < 0.001$, $p < 0.01$, $p < 0.05$ respectively for U251; $p < 0.001$ for T98G cells). On the contrary, this effect was not observed for GemC$_{12}$ and GemC$_{12}$-LNC suggesting that the internalization of these two drugs does not rely on the same adenosine transporters as the commercial drug GemHCl. A similar behavior was also observed for 9L-LacZ (especially at 0.1 μM; Fig. 1C) and U-87 MG cells (Fig. 1D), but to a much lesser extent. Indeed, 9L-LacZ cells are much more sensitive to gemcitabine in all its three forms compared to the other cell lines studied, showing < 35% survival starting from 0.1 μM in the absence of Dyp (Fig. S1). At this concentration, GemHCl is significantly more cytotoxic than GemC$_{12}$ and GemC$_{12}$-LNC ($p < 0.01$, $p < 0.001$ respectively), while at lower or higher concentrations no significant difference is observed between the groups. When the transporter inhibitor is added, GemHCl seems less cytotoxic but not in a significant way (Fig. 1C), meaning that in this cell line other transporters are probably involved in the cellular drug uptake. On the other side, U-87 MG cells are less sensitive to GemHCl in the examined concentration range, decreasing the influence of the inhibitor on the drug cytotoxicity (Fig. 1D). Moreover, it has been previously shown that adenosine analogue uptake is only partially inhibited by Dyp in U-87 MG, possibly because of an altered hENT phenotype [41]. Overall, our results are in accordance with other studies performed on non-GBM cell lines who reported that gemcitabine derivatives, alone or in nanoparticles, are less sensitive to the hENT1 inhibition than gemcitabine HCl. The improved lipophilicity of Gem derivatives could enhance intracellular uptake *via* passive pathways or endocytosis thus improving growth inhibition effects [42–44]. However interestingly, for all cell lines tested in this work, the cytotoxic action of GemC$_{12}$ and GemC$_{12}$-LNC seem potentiated by the presence of Dyp. As hENT are bidirectional, the net drug uptake is represented by the combined contributions of NT-mediated influx and efflux [38,45]. We hypothesize that the drug effect potentiation could then be correlated to the presence and action of inwardly directed hCNT, which could also be responsible for GemC$_{12}$ and GemC$_{12}$-LNC uptake in these cell lines.

3.2. Internalization studies of LNC into GBM cell lines

Garcion et al. and Paillard et al. [46,47] have previously demonstrated, by using the F98 glioma cell line, that LNC internalization is mediated through an active, saturable, clathrin/caveolae-independent endocytosis mechanism involving endogenous cholesterol. To test whether the presence of GemC$_{12}$ at the interface of the LNCs could influence its cellular uptake, we performed internalization studies using LNC labeled with the fluorescent dye DiD using flow cytometry (FACS) and fluorescence microscopy. Therefore, we have compared the capacity of DiD-LNC and DiD-GemC$_{12}$-LNC to enter U251, T98G, 9L-LacZ and U-87 MG glioma cells after 1 h or 8 h of incubation at 4 °C or 37 °C. At 4 °C, when energy consumption and active transport processes are minimal [48], increased fluorescence was observed in cells treated with GemC$_{12}$-LNC compared to unloaded LNC (Fig. 2). However, this difference is only significant in 9L-LacZ after 8 h (**$p < 0.01$) and in U-87 MG cells after 1 h and 8 h (*$p < 0.05$). At 37 °C we observed a significant difference between unloaded LNC and GemC$_{12}$-LNC after 8 h in all the cell lines (**$p < 0.01$ for U251, T98G; ***$p < 0.001$ for U-
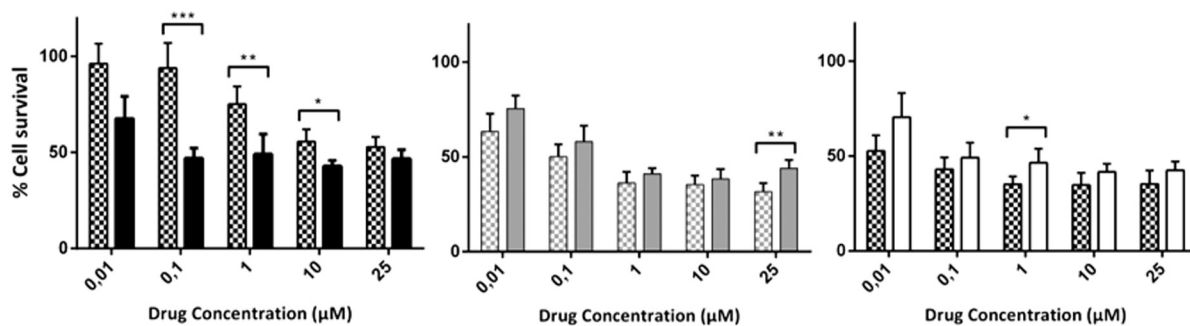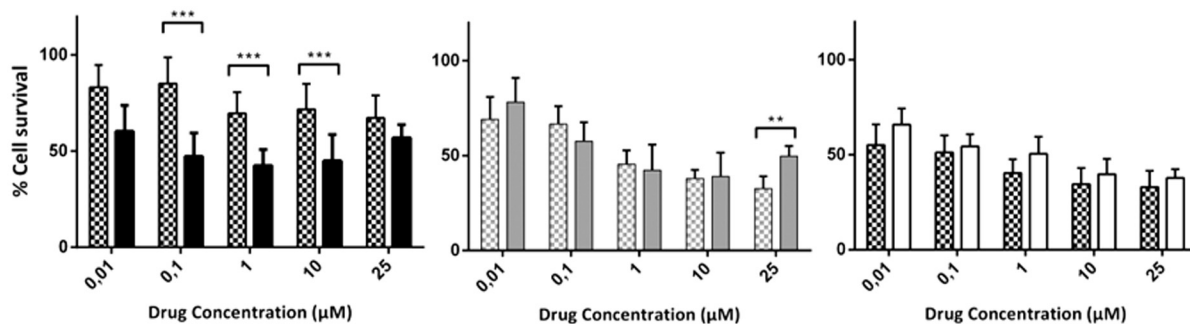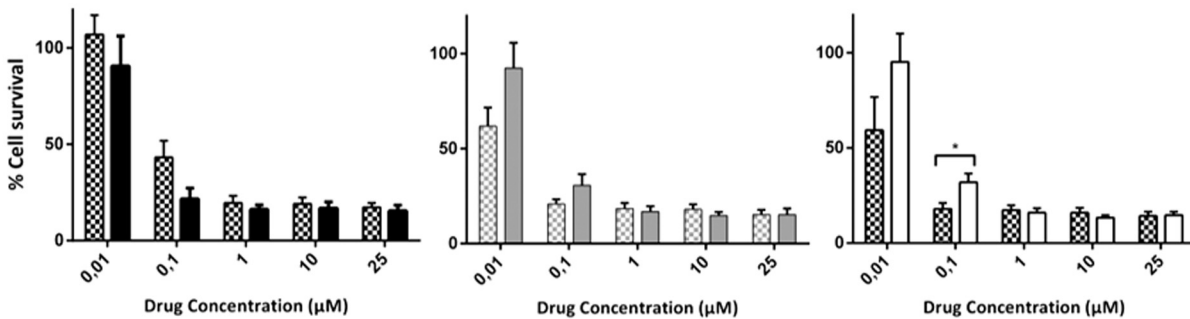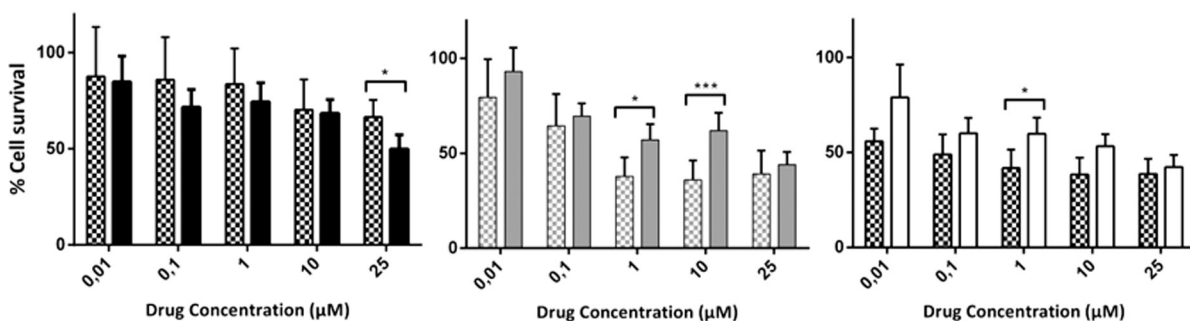
Fig. 1. *In vitro* cytotoxicity studies on (**A**) U251, (**B**) T98G, (**C**) 9L-LacZ, and (**D**) U-87 MG glioma cells. Crystal violet staining after 48 h of incubation of different concentrations of GemHCl (black bar), $GemC_{12}$ (gray bar) or $GemC_{12}$-LNC (white bar) with or without 10 μM of hENT1 transporter inhibitor dypiridamole (squared pattern or filled pattern, respectively). Data are presented as percentage of cell survival (untreated cells assumed as 100%) (mean ± SD, N = 3 n = 18). ***p < 0.001, **p < 0.01, *p < 0.05 by Kruskal-Wallis test + Dunn multiple comparison post-test. (For interpretation of the references to colour in this figure legend, the reader is referred to the web version of this article.)
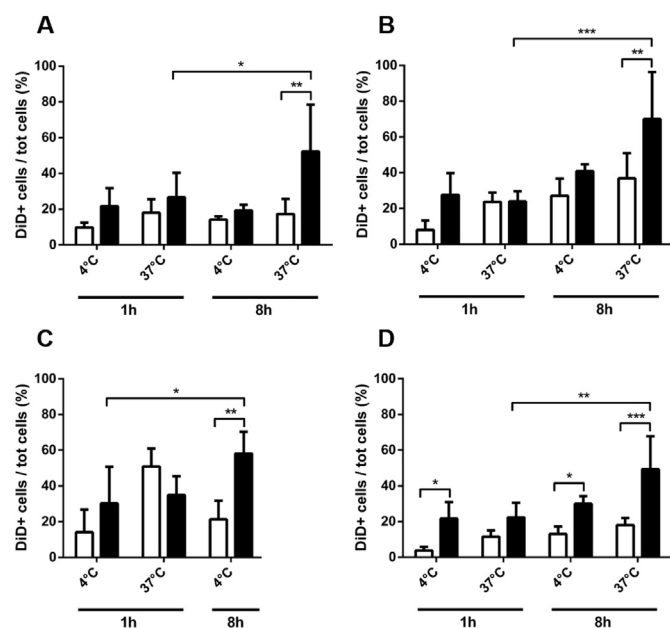
Fig. 2. *In vitro* cellular uptake studies: flow cytometry analysis after 1 h or 8 h incubation with fluorescent-labeled (DiD) unloaded LNC (white bars) or GemC$_{12}$-LNC (1.21 mg/mL LNC, 100 μM GemC$_{12}$; black bars) of (**A**) U251, (**B**) T98G, (**C**) 9L-LacZ, and (**D**) U-87 MG glioma cells at 4 and 37 °C. Percentage of fluorescent cells relative to all cells measured by flow cytometry normalized to each control (HBSS). ***$p < 0.001$, **$p < 0.01$, *$p < 0.05$ by two-way ANOVA test with Bonferroni post-test (mean ± SD, N = 3 n = 3).

87 MG respectively) except 9L-LacZ where, at this concentration, both conditions are cytotoxic (data not shown). As it has been previously demonstrated that DiD labelling is irreversible and can be used to confirm the uptake of the LNC in the cells [49], we used fluorescent microscopy to qualitatively confirm the nanocarrier uptake. Fig. 3, which represents the U-87 MG cells following 8 h of incubation with DiD-LNC and DiD-GemC$_{12}$-LNC, shows absence of DiD signal in the proximity of the cell nuclei for the unloaded LNC at 4 °C and low DiD signal at 37 °C. Its detection increases for the DiD-GemC$_{12}$-LNC, especially at 37 °C confirming that cellular uptake of the drug-loaded nanocarrier is mediated through active transport. These results are in accordance with those of the cytotoxicity studies.

3.3. Mid-term and long-term tolerability of GemC$_{12}$-LNC in mouse brain

We previously reported that, after one week of exposure, no significant inflammation was observed in the GemC$_{12}$-LNC group compared to the control groups (PBS and unloaded LNC), while some singular apoptotic cells and slight microglia activation were observed [29]. However, it is known that neuroinflammation following injury or administration of implants into the brain can last for a much longer

period, and the main actors in this response are activated microglia and astrocytes. The latter can form a gliotic scar, creating a barrier between the affected and the unaffected brain areas [50]. Once the inflammatory response recedes, the tissue is repaired and the damaged areas strengthened, while the cells restore their normal morphology [50].

Therefore, to evaluate the influence of prolonged exposure to GemC$_{12}$-LNC gel in the mouse brain, we evaluated its tolerability after 2 and 6 months. During the study, none of the animals showed behavioral changes, apparent neurological deficits or body weight loss. All the brains had normal morphology and no apparent lesions were visible immediately after extraction and fixation. While sectioning, the hole corresponding to the administration site was easily visualized in almost all the brains. Fig. 4 shows brain sections of the PBS and GemC$_{12}$-LNC treated groups. After two months, no increased inflammation, apoptosis or microglia activation was observed in the GemC$_{12}$-LNC group compared to the controls in proximity to the site of injection. Interestingly, in two of the animals treated with GemC$_{12}$-LNC hydrogel, a cavity was observed below the injection site, which could correspond to the space occupied by the hydrogel (Fig. S2). Around this formed cavity the presence of activated microglia was slightly increased compared to the controls. Their presence could have resulted from the slow degradation of the hydrogel and, therefore, a longer contact of the foreign body (hydrogel) with the tissue compared to the other groups. Indeed, it has been previously shown that slower rates of hydrogel degradation can lead to higher microglial activation as these cells can phagocytose the degradation products [50].

After six months, no increase in inflammation, apoptosis or microglia activation was observed in the GemC$_{12}$-LNC group compared to the controls.

It is important to note that unloaded LNC and GemC$_{12}$ groups exhibited similar results (normal shape, no lesion, no inflammation, no apoptosis; data not shown).

Our results are in accordance with previous tolerability studies on controlled release systems, which showed a typical and mild foreign body reaction being resolved 2 months after implantation [51]. In conclusion, the GemC$_{12}$-LNC can be considered as well tolerated in mouse brain and therefore suitable for local administration into the brain.

3.4. Anti- tumor efficacy of GemC$_{12}$-LNC hydrogel after intratumoral administration in an orthotopic U-87 MG human glioblastoma

To test the antitumor efficacy of the GemC$_{12}$-LNC hydrogel, the U-87 MG human xenograft orthotopic model in nude mice was chosen for its wide use as a preclinical model, good reproducibility, reliable growth and disease progression [52]. These tumors are non-infiltrative, with a well demarcated tumor mass visible both by MRI images and Hematoxylin & Eosin stained sections [37], but present a subpopulation of cancer stem-like cells with self-propagating potential [53]. These features make it a good model for testing the antitumor efficacy after local delivery of a drug into the tumor or in the tumor resection cavity.
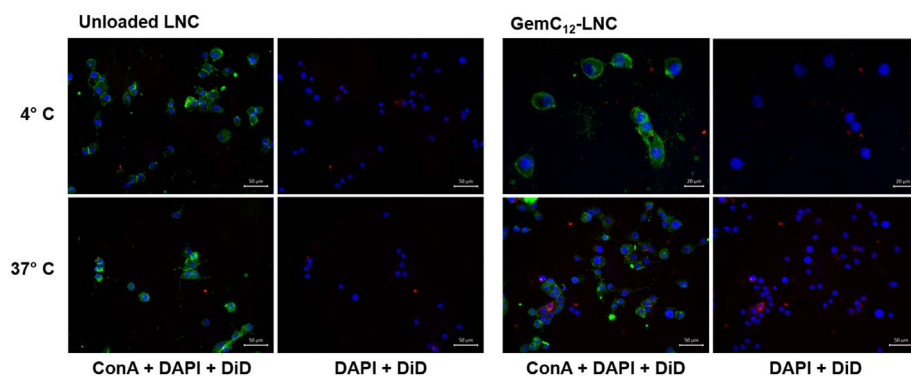

Fig. 3. Fluorescence microscopy images of U-87 MG glioma cells after 8 h incubation with fluorescent-labeled (DiD) unloaded LNC or GemC$_{12}$-LNC at 4 °C and 37 °C. Blue: cells nuclei (DAPI); Green: cell membranes (Concanavalin A, Alexa Fluor® 488 Conjugate); Red: LNC (DiD). Microscope images: 20 × (scale bar 50 μm) or 40 × (scale bar 20 μm). (For interpretation of the references to colour in this figure legend, the reader is referred to the web version of this article.)
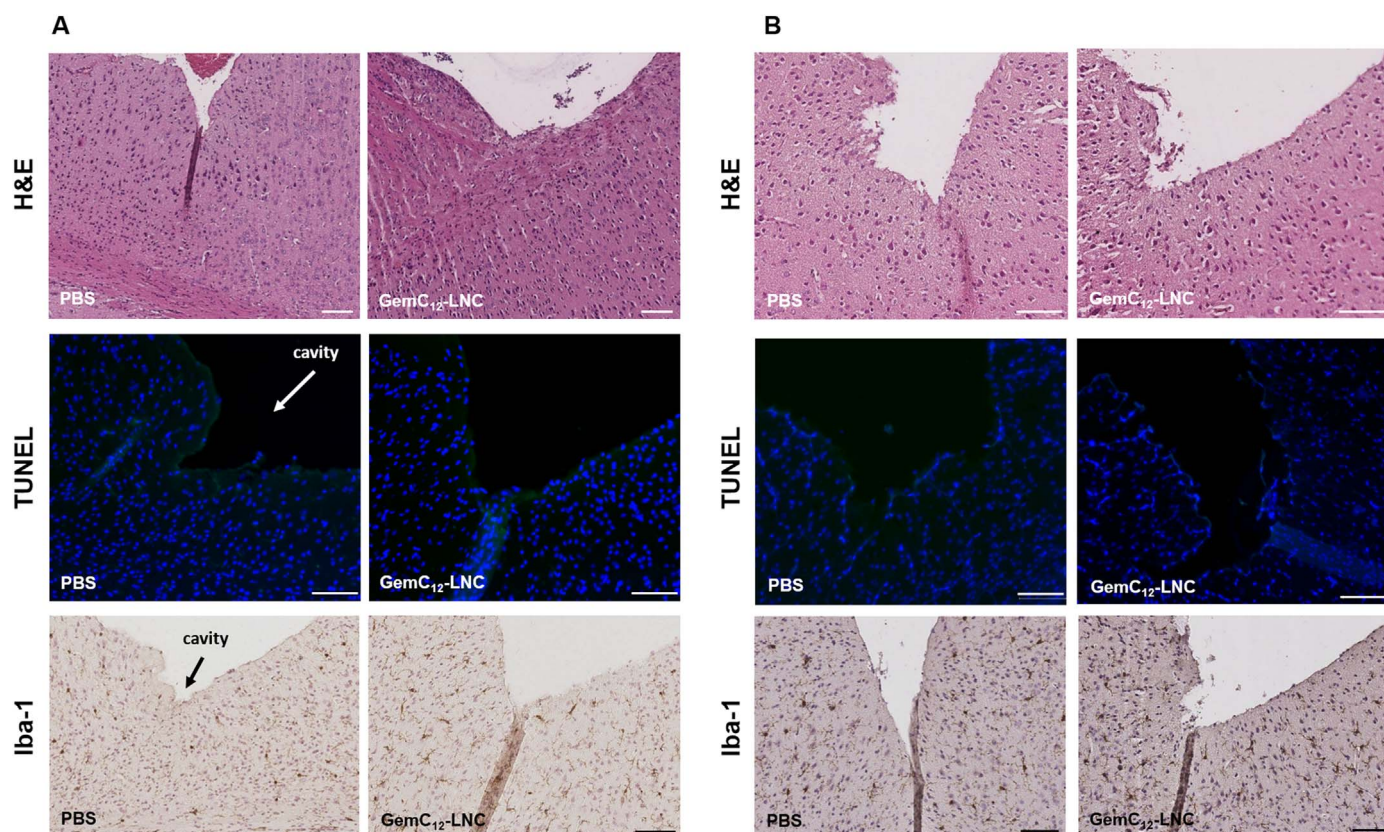
Fig. 4. *In vivo* mid-term (**A**) and long-term (**B**) tolerability assay. Evaluation of the inflammatory response (Hematoxylin & Eosin staining, upper panel), cell apoptosis (TUNEL assay, mid panel) and microglia activation (Iba-1 staining, lower panel) in the brain tissue 2 months (mid-term) or 6 months (long-term) after local injection of PBS and GemC$_{12}$-LNC. Scale bar: 100 μm (n = 3–5). TUNEL assay: living nuclei (Blue, DAPI); apoptotic cells (Green, TUNEL). Scale bar: 100 μm. (For interpretation of the references to colour in this figure legend, the reader is referred to the web version of this article.)

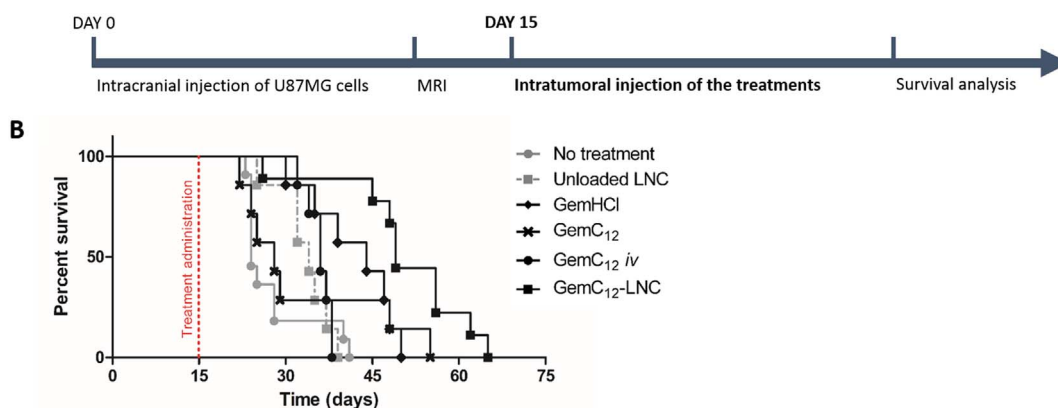**Fig. 5.** (**A**) Time schedule of the anti-tumor efficacy studies using an orthotopic U-87 MG human glioblastoma tumor model; (**B**) Kaplan-Meier survival curves for animals treated intratumorally with this model. Drug dose administered: 3 mg/kg (n = 7–11 for all groups).

U-87 MG cells were injected at the border between the striatum and the cortex of nude mice using a stereotactic frame and the tumor was visualized by MRI. To evaluate the antitumor efficacy of the hydrogel and its capacity to slow down tumor recurrences, treatments were administered intratumorally by stereotactic injection at day 15 post-tumor inoculation (Fig. 5).

The survival data of the different groups are summarized in Table 1 and Kaplan-Meier survival curves are shown in Fig. 5. In this orthotopic model, the median survival of the GemC$_{12}$-LNC treated mice was compared to all the other groups and a significant improvement in the median survival of mice treated with the hydrogel was observed

compared to the other treatments. Interestingly, no differences were observed between the intravenous and intratumoral administration of the free drug GemC$_{12}$, while intratumoral administration of GemC$_{12}$-LNC significantly prolonged animal survival compared to both these groups. These results, which are in accordance with the short-term efficacy studies we have previously reported using GemC$_{12}$-LNC hydrogel in a subcutaneous GBM xenograft tumor model [29], might be explained by the sustained continuous drug release obtained by a gel formulation compared to the unloaded liquid form, and they confirm the rationale for the use of Gem derivatives as a local delivery strategy for GBM. Recently, Gaudin et al. also reported an increased survival

Table 1

***In vivo* efficacy studies:** median survival (days) of animals treated intratumorally at day 15 post-cell inoculation (orthotopic model) or locally treated in the tumor resection cavity at day 13 post-cell inoculation (resection model).

Tumor model	Treatment	*n*	Survival time (days)		Mantel Cox test (each *vs* GemC$_{12}$-LNC)
			Range	Median	
Orthotopic model	No treatment	11	23–41	24	***
	Unloaded LNC	7	25–39	34	***
	GemHCl	7	30–50	44	*
	GemC$_{12}$	7	22–55	28	*
	GemC$_{12}$*iv*	7	32–38	36	**
	GemC$_{12}$-LNC	9	26–65	49	
Orthotopic resection model	No treatment	10	29–45	35.5	**
	Unloaded LNC	7	29–51	38	*
	GemHCl	7	29–53	37	*
	GemC$_{12}$	7	28–92	61	n.s.
	GemC$_{12}$-LNC	7	32–92	62	

n: number of animals per group; Mantel Cox test: survival curve comparison between each control group and the GemC$_{12}$-LNC hydrogel (n.s. *p* > 0.05).

*** *p* < 0.001.
** *p* < 0.01.
* *p* < 0.05.

time of animals treated with squaneoyl-Gemcitabine nanoparticles compared to free drug after local administration by CED in an orthotopic RG2 GBM model [54].

3.5. Anti-tumor efficacy of GemC$_{12}$-LNC hydrogel after perisurgical administration in the U-87 MG tumor resection cavity

To better mimic the local delivery clinical scenario, a second anti-tumor efficacy study was performed after perisurgical administration of GemC$_{12}$-LNC within the tumor resection cavity (Fig. 6A). For this last purpose, we used a subtotal resection model that we recently developed and validated [37]. Here, U-87 MG cells were injected at the border between the striatum and the cortex of nude mice using a stereotactic frame and the tumor was visualized by MRI. At day 13 post-tumor inoculation, the brain region around the tumor was defined by a 2 mm diameter biopsy punch that was inserted at a depth of 3 mm from the skull border. The resulting explant was then aspirated leading to a resection cavity able to host 5 μL of GemC$_{12}$-LNC hydrogel, corresponding to 3 mg/kg (Fig. 6B; Video S1). Recurrence of the tumors, which lead to mouse death, were observed in all animals where a primary tumor had been detected by MRI but they appeared at different time points depending on the treatment administered (Fig. 6C).

As for the previous model, the median survival of the GemC$_{12}$-LNC treated mice was compared to all the other groups (Table 1). Significant improvement in the median survival of mice, and therefore slowdown of tumor recurrences formations, was observed in groups treated with GemC$_{12}$ and GemC$_{12}$-LNC hydrogel compared to the untreated, unloaded LNC and GemHCl-treated animals (Fig. 6D). Interestingly, the curves of the GemC$_{12}$ and GemC$_{12}$-LNC groups almost overlap in the orthotopic resection tumor model, while in the orthotopic non-resected tumor model a significant difference between the curves is observed (*p* < 0.05). This different result could be explained by the tumor microenvironment *vs* post-resection tumor microenvironment characteristics [55], the immunostimulatory capacities of Gemcitabine [56],

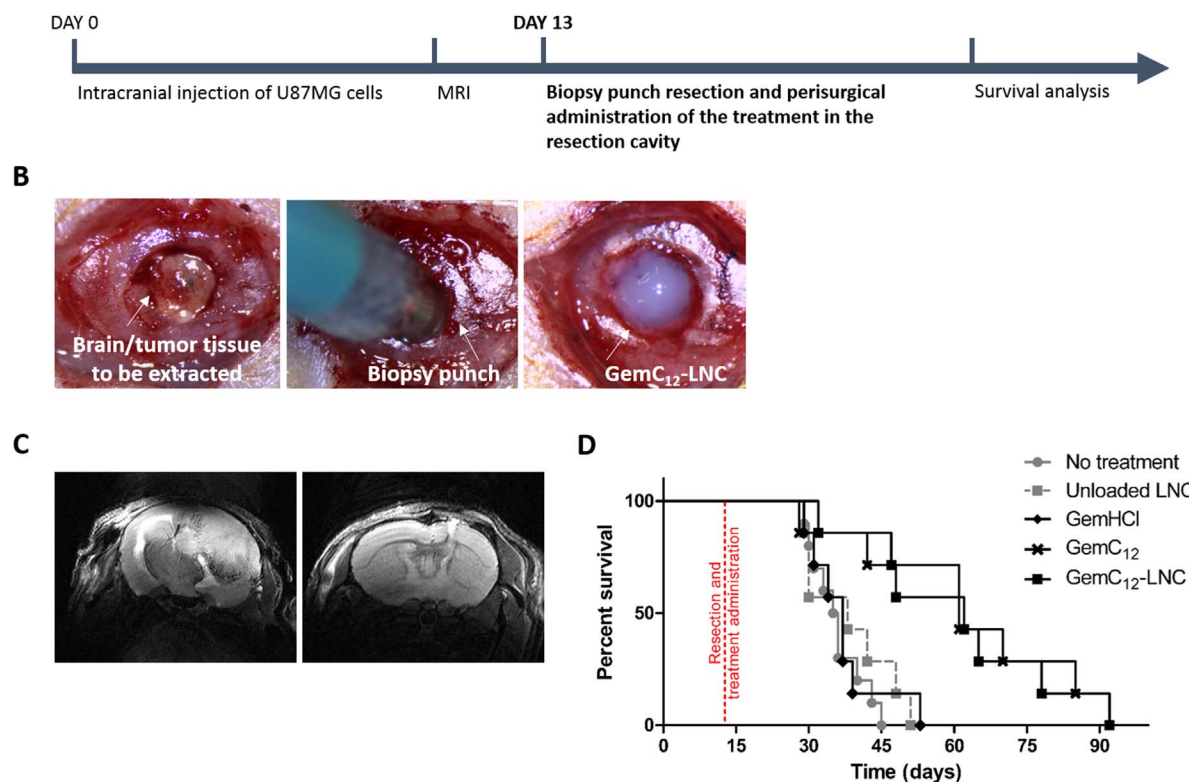**A IN VIVO EFFICACY ON RESECTION MODEL OF ORTHOTOPIC U-87 MG HUMAN GBM TUMOR:**

Fig. 6. (**A**) Time schedule of the anti-tumor efficacy studies using a resection model of orthotopic U-87 MG human glioblastoma tumor model; (**B**) Images taken during the tumor resection surgeries and treatment administration: tumor tissue visible within the 2 × 2 mm cranial window (left), biopsy punch twisting (middle) followed by aspiration. GemC$_{12}$-LNC hydrogel (5 μL) injected into the resection cavity, and filling it completely (right). (**C**) Axial (T$_2$-weighted) images of mouse brain following resection: untreated (day 31 post-resection, left) and treated with GemC$_{12}$-LNC (day 61 post-resection, right). (**D**) Kaplan-Meier survival curves for animals treated locally in the resection cavity. Drug dose administered: 3 mg/kg (*n* = 7–11 for all groups).

and possibly different humoral adaptive and innate immune response of the animals in our two orthotopic tumor models [57]. For example, Sasso et al. have recently demonstrated the targeting capacity of GemC$_{12}$-LNC towards the monocytic-myeloid derived suppressor cells (MDSCs) in lymphoma and melanoma mouse models [58]. MDSCs are a heterogeneous population of granulocytic and myeloid cells, highly present in GBM patients, able to accumulate in the tumor-bearing host to support glioma growth, invasion, and vascularization, and differentially mediating immunosuppression depending on their stage [59–61]. The targeted action of GemC$_{12}$-LNC on these cells could potentially reduce the tumor-associated immunosuppression in the orthotopic tumor model (where the tumor microenvironment is not affected by the resection procedure), thus increasing its efficacy compared to the free drug. This assumption will be subject of further studies in more appropriate immunological rodent models.

4. Conclusions

The objective of this work was to test the cytotoxicity, mid- and long-term tolerability and efficacy of GemC$_{12}$-LNC nanomedicine hydrogel on GBM. We demonstrated that the different cytotoxic effects observed on GBM cells lines for GemC$_{12}$-LNC and the commercial drug GemHCl might be due to different cell transport mechanisms (different adenosine transporters, endocytosis). The GemC$_{12}$-LNC hydrogel is well tolerated in mouse brain after 2 and 6 months of exposure, suggesting that this system is suitable for an application in the brain. Intratumoral administration of the hydrogel in an orthotopic human xenograft GBM model showed a significant increase in the animals' survival compared to the controls. Moreover, using a reproducible U87 GBM tumor resection technique, we demonstrated that GemC$_{12}$-LNC hydrogel slows down recurrences formation after perisurgical administration in the resection cavity. To our knowledge, it is the first time that this surgical resection procedure, which allows to mimic the clinical setting, is used to test local delivery of anticancer drugs in orthotopic GBM mouse models. In conclusion, GemC$_{12}$-LNC nanomedicine-based hydrogel could be considered as a promising strategy for the local treatment of GBM, although further studies need to be performed to show its efficacy in other animal models, and in synergy with other chemotherapeutic agents and/or radiotherapy.

Acknowledgments

References

[1] E.C. Holland, Glioblastoma multiforme: the terminator, Proc. Natl. Acad. Sci. U. S. A. 97 (2000) 6242–6244.

[2] D.N. Louis, A. Perry, G. Reifenberger, A. von Deimling, D. Figarella-Branger, W.K. Cavenee, H. Ohgaki, O.D. Wiestler, P. Kleihues, D.W. Ellison, The 2016 World Health Organization classification of tumors of the central nervous system: a summary, Acta Neuropathol. 131 (2016) 803–820.

[3] R.L. Yong, R.R. Lonser, Surgery for glioblastoma multiforme: striking a balance, World Neurosurg. 76 (2011) 528–530.

[4] K.R. Yabroff, L. Harlan, C. Zeruto, J. Abrams, B. Mann, Patterns of care and survival for patients with glioblastoma multiforme diagnosed during 2006, Neuro-Oncology 14 (2012) 351–359.

[5] R. Stupp, M. Brada, M.J. van den Bent, J.C. Tonn, G. Pentheroudakis, High-grade glioma: ESMO Clinical Practice Guidelines for diagnosis, treatment and follow-up, Ann. Oncol. 25 (Suppl. 3) (2014) iii93–iii101.

[6] F.H. Hochberg, A. Pruitt, Assumptions in the radiotherapy of glioblastoma, Neurology 30 (1980) 907–911.

[7] S. Roy, D. Lahiri, T. Maji, J. Biswas, Recurrent glioblastoma: where we stand, South Asian J. Cancer 4 (2015) 163–173.

[8] R. Stupp, M.E. Hegi, W.P. Mason, M.J. van den Bent, M.J. Taphoorn, R.C. Janzer, S.K. Ludwin, A. Allgeier, B. Fisher, K. Belanger, P. Hau, A.A. Brandes, J. Gijtenbeek, C. Marosi, C.J. Vecht, K. Mokhtari, P. Wesseling, S. Villa, E. Eisenhauer, T. Gorlia, M. Weller, D. Lacombe, J.G. Cairncross, R.O. Mirimanoff, Effects of radiotherapy with concomitant and adjuvant temozolomide versus radiotherapy alone on survival in glioblastoma in a randomised phase III study: 5-year analysis of the EORTC-NCIC trial, Lancet Oncol. 10 (2009) 459–466.

[9] N.R. Smoll, K. Schaller, O.P. Gautschi, Long-term survival of patients with glioblastoma multiforme (GBM), J. Clin. Neurosci. 20 (2013) 670–675.

[10] T. Yamahara, Y. Numa, T. Oishi, T. Kawaguchi, T. Seno, A. Asai, K. Kawamoto, Morphological and flow cytometric analysis of cell infiltration in glioblastoma: a comparison of autopsy brain and neuroimaging, Brain Tumor Pathol. 27 (2010) 81–87.

[11] T. Denysenko, L. Gennero, M.A. Roos, A. Melcarne, C. Juenemann, G. Faccani, I. Morra, G. Cavallo, S. Reguzzi, G. Pescarmona, A. Ponzetto, Glioblastoma cancer stem cells: heterogeneity, microenvironment and related therapeutic strategies, Cell Biochem. Funct. 28 (2010) 343–351.

[12] D. Treister, S. Kingston, K.E. Hoque, M. Law, M.S. Shiroishi, Multimodal magnetic resonance imaging evaluation of primary brain tumors, Semin. Oncol. 41 (2014) 478–495.

[13] S. Osuka, E.G. Van Meir, Overcoming therapeutic resistance in glioblastoma: the way forward, J. Clin. Invest. 127 (2017) 415–426.

[14] D.M. Patel, N. Agarwal, K.L. Tomei, D.R. Hansberry, I.M. Goldstein, Optimal timing of whole-brain radiation therapy following craniotomy for cerebral malignancies, World Neurosurg. 84 (2015) 412–419.

[15] J.R. Silber, M.S. Bobola, A. Blank, M.C. Chamberlain, O(6)-methylguanine-DNA methyltransferase in glioma therapy: promise and problems, Biochim. Biophys. Acta 1826 (2012) 71–82.

[16] N.R. Parker, A.L. Hudson, P. Khong, J.F. Parkinson, T. Dwight, R.J. Ikin, Y. Zhu, Z.J. Cheng, F. Vafaee, J. Chen, H.R. Wheeler, V.M. Howell, Intratumoral heterogeneity identified at the epigenetic, genetic and transcriptional level in glioblastoma, Sci Rep 6 (2016) 22477.

[17] H. Okura, C.A. Smith, J.T. Rutka, Gene therapy for malignant glioma, Mol. Cell. Ther. 2 (2014) 21.

[18] A. Tivnan, T. Heilinger, E.C. Lavelle, J.H. Prehn, Advances in immunotherapy for the treatment of glioblastoma, J. Neuro-Oncol. 131 (2017) 1–9.

[19] A. Mangraviti, D. Gullotti, B. Tyler, H. Brem, Nanobiotechnology-based delivery strategies: new frontiers in brain tumor targeted therapies, J. Control. Release 240 (2016) 443–453.

[20] R. Karim, C. Palazzo, B. Evrard, G. Piel, Nanocarriers for the treatment of glioblastoma multiforme: current state-of-the-art, J. Control. Release 227 (2016) 23–37.

[21] A. Burgess, K. Shah, O. Hough, K. Hynynen, Focused ultrasound-mediated drug delivery through the blood-brain barrier, Expert. Rev. Neurother. 15 (2015) 477–491.

[22] J. Bianco, C. Bastiancich, A. Jankovski, A. des Rieux, V. Preat, F. Danhier, On glioblastoma and the search for a cure: where do we stand? Cell. Mol. Life Sci. 74 (13) (2017) 2451–2466.

[23] M. Westphal, Z. Ram, V. Riddle, D. Hilt, E. Bortey, Gliadel wafer in initial surgery for malignant glioma: long-term follow-up of a multicenter controlled trial, Acta Neurochir. 148 (2006) 269–275 (discussion 275).

[24] P. Menei, L. Capelle, J. Guyotat, S. Fuentes, R. Assaker, B. Bataille, P. Francois, D. Dorwling-Carter, P. Paquis, L. Bauchet, F. Parker, J. Sabatier, N. Faisant, J.P. Benoit, Local and sustained delivery of 5-fluorouracil from biodegradable microspheres for the radiosensitization of malignant glioma: a randomized phase II trial, Neurosurgery 56 (2005) 242–248 (discussion 242-248).

[25] C. Bastiancich, P. Danhier, V. Preat, F. Danhier, Anticancer drug-loaded hydrogels as drug delivery systems for the local treatment of glioblastoma, J. Control. Release 243 (2016) 29–42.

[26] D.A. Bota, A. Desjardins, J.A. Quinn, M.L. Affronti, H.S. Friedman, Interstitial chemotherapy with biodegradable BCNU (Gliadel) wafers in the treatment of malignant gliomas, Ther. Clin. Risk Manag. 3 (2007) 707–715.

[27] M. Westphal, D.C. Hilt, E. Bortey, P. Delavault, R. Olivares, P.C. Warnke, I.R. Whittle, J. Jaaskelainen, Z. Ram, A phase 3 trial of local chemotherapy with biodegradable carmustine (BCNU) wafers (Gliadel wafers) in patients with primary malignant glioma, Neuro-Oncology 5 (2003) 79–88.

[28] P.C. McGovern, E. Lautenbach, P.J. Brennan, R.A. Lustig, N.O. Fishman, Risk factors for postcraniotomy surgical site infection after 1,3-bis (2-chloroethyl)-1-nitrosourea (Gliadel) wafer placement, Clin. Infect. Dis. 36 (2003) 759–765.

[29] C. Bastiancich, K. Vanvarenberg, B. Ucakar, M. Pitorre, G. Bastiat, F. Lagarce, V. Preat, F. Danhier, Lauroyl-gemcitabine-loaded lipid nanocapsule hydrogel for the treatment of glioblastoma, J. Control. Release 225 (2016) 283–293.

[30] T. Fourniols, L.D. Randolph, A. Staub, K. Vanvarenberg, J.G. Leprince, V. Preat, A. des Rieux, F. Danhier, Temozolomide-loaded photopolymerizable PEG-DMA-based hydrogel for the treatment of glioblastoma, J. Control. Release 210 (2015) 95–104.

[31] J.B. Wolinsky, Y.L. Colson, M.W. Grinstaff, Local drug delivery strategies for cancer treatment: gels, nanoparticles, polymeric films, rods, and wafers, J. Control. Release 159 (2012) 14–26.

[32] B. Heurtault, P. Saulnier, B. Pech, J.E. Proust, J.P. Benoit, A novel phase inversion-based process for the preparation of lipid nanocarriers, Pharm. Res. 19 (2002) 875–880.

[33] E. Moysan, Y. Gonzalez-Fernandez, N. Lautram, J. Bejaud, G. Bastiat, J.P. Benoit, An innovative hydrogel of gemcitabine-loaded lipid nanocapsules: when the drug is

a key player of the nanomedicine structure, Soft Matter 10 (2014) 1767–1777.

[34] N. Wauthoz, G. Bastiat, E. Moysan, A. Cieslak, K. Kondo, M. Zandecki, V. Moal, M.C. Rousselet, J. Hureaux, J.P. Benoit, Safe lipid nanocapsule-based gel technology to target lymph nodes and combat mediastinal metastases from an orthotopic non-small-cell lung cancer model in SCID-CB17 mice, Nanomedicine 11 (2015) 1237–1245.

[35] R.L. Alexander, B.T. Greene, S.V. Torti, G.L. Kucera, A novel phospholipid gemcitabine conjugate is able to bypass three drug-resistance mechanisms, Cancer Chemother. Pharmacol. 56 (2005) 15–21.

[36] F. Danhier, K. Messaoudi, L. Lemaire, J.P. Benoit, F. Lagarce, Combined anti-Galectin-1 and anti-EGFR siRNA-loaded chitosan-lipid nanocapsules decrease temozolomide resistance in glioblastoma: in vivo evaluation, Int. J. Pharm. 481 (2015) 154–161.

[37] J. Bianco, C. Bastiancich, N. Joudiou, B. Gallez, A. des Rieux, F. Danhier, Novel model of orthotopic U-87 MG glioblastoma resection in athymic nude mice, J. Neurosci. Methods 284 (2017) 96–102.

[38] J.R. Mackey, R.S. Mani, M. Selner, D. Mowles, J.D. Young, J.A. Belt, C.R. Crawford, C.E. Cass, Functional nucleoside transporters are required for gemcitabine influx and manifestation of toxicity in cancer cell lines, Cancer Res. 58 (1998) 4349–4357.

[39] V.L.D.J. Sun, C.E. Cass, M.B. Sawyer, Inhibition of nucleoside transporters by tyrosine kinase inhibitors and its effects on chemotherapy efficacy, Cancer Cell Microenviron. 1 (2014) e389.

[40] J. Rieger, S. Durka, J. Streffer, J. Dichgans, M. Weller, Gemcitabine cytotoxicity of human malignant glioma cells: modulation by antioxidants, BCL-2 and dexamethasone, Eur. J. Pharmacol. 365 (1999) 301–308.

[41] S.Y. Cho, J. Polster, J.M. Engles, J. Hilton, E.H. Abraham, R.L. Wahl, In vitro evaluation of adenosine 5′-monophosphate as an imaging agent of tumor metabolism, J. Nucl. Med. 47 (2006) 837–845.

[42] X.M. Tao, J.C. Wang, J.B. Wang, Q. Feng, S.Y. Gao, L.R. Zhang, Q. Zhang, Enhanced anticancer activity of gemcitabine coupling with conjugated linoleic acid against human breast cancer in vitro and in vivo, Eur. J. Pharm. Biopharm. 82 (2012) 401–409.

[43] P.D. Lansakara, B.L. Rodriguez, Z. Cui, Synthesis and in vitro evaluation of novel lipophilic monophosphorylated gemcitabine derivatives and their nanoparticles, Int. J. Pharm. 429 (2012) 123–134.

[44] R.D. Dubey, A. Saneja, P.K. Gupta, P.N. Gupta, Recent advances in drug delivery strategies for improved therapeutic efficacy of gemcitabine, Eur. J. Pharm. Sci. 93 (2016) 147–162.

[45] D.S. Gesto, N.M. Cerqueira, P.A. Fernandes, M.J. Ramos, Gemcitabine: a critical nucleoside for cancer therapy, Curr. Med. Chem. 19 (2012) 1076–1087.

[46] E. Garcion, A. Lamprecht, B. Heurtault, A. Paillard, A. Aubert-Pouessel, B. Denizot, P. Menei, J.P. Benoit, A new generation of anticancer, drug-loaded, colloidal vectors reverses multidrug resistance in glioma and reduces tumor progression in rats, Mol. Cancer Ther. 5 (2006) 1710–1722.

[47] A. Paillard, F. Hindre, C. Vignes-Colombeix, J.P. Benoit, E. Garcion, The importance of endo-lysosomal escape with lipid nanocapsules for drug subcellular

[48] K. Sugano, M. Kansy, P. Artursson, A. Avdeef, S. Bendels, L. Di, G.F. Ecker, B. Faller, H. Fischer, G. Gerebtzoff, H. Lennernaes, F. Senner, Coexistence of passive and carrier-mediated processes in drug transport, Nat. Rev. Drug Discov. 9 (2010) 597–614.

[49] G. Bastiat, C.O. Pritz, C. Roider, F. Fouchet, E. Lignieres, A. Jesacher, R. Glueckert, M. Ritsch-Marte, A. Schrott-Fischer, P. Saulnier, J.P. Benoit, A new tool to ensure the fluorescent dye labeling stability of nanocarriers: a real challenge for fluorescence imaging, J. Control. Release 170 (2013) 334–342.

[50] K.B. Bjugstad, K. Lampe, D.S. Kern, M. Mahoney, Biocompatibility of poly(ethylene glycol)-based hydrogels in the brain: an analysis of the glial response across space and time, J. Biomed. Mater. Res. A 95 (2010) 79–91.

[51] E. Fournier, C. Passirani, N. Colin, S. Sagodira, P. Menei, J.P. Benoit, C.N. Montero-Menei, The brain tissue response to biodegradable poly(methylidene malonate 2.1.2)-based microspheres in the rat, Biomaterials 27 (2006) 4963–4974.

[52] V.L. Jacobs, P.A. Valdes, W.F. Hickey, J.A. De Leo, Current review of in vivo GBM rodent models: emphasis on the CNS-1 tumour model, ASN Neuro 3 (2011) e00063.

[53] L. Qiang, Y. Yang, Y.J. Ma, F.H. Chen, L.B. Zhang, W. Liu, Q. Qi, N. Lu, L. Tao, X.T. Wang, Q.D. You, Q.L. Guo, Isolation and characterization of cancer stem like cells in human glioblastoma cell lines, Cancer Lett. 279 (2009) 13–21.

[54] A. Gaudin, E. Song, A.R. King, J.K. Saucier-Sawyer, R. Bindra, D. Desmaele, P. Couvreur, W.M. Saltzman, PEGylated squalenoyl-gemcitabine nanoparticles for the treatment of glioblastoma, Biomaterials 105 (2016) 136–144.

[55] O. Okolie, J.R. Bago, R.S. Schmid, D.M. Irvin, R.E. Bash, C.R. Miller, S.D. Hingtgen, Reactive astrocytes potentiate tumor aggressiveness in a murine glioma resection and recurrence model, Neuro-Oncology 18 (2016) 1622–1633.

[56] L. Zitvogel, A. Tesniere, L. Apetoh, F. Ghiringhelli, G. Kroemer, Immunological aspects of anticancer chemotherapy, Bulletin de l'Academie nationale de medecine 192 (2008) 1469–1487 (discussion 1487-1469).

[57] I. Szadvari, O. Krizanova, P. Babula, Athymic nude mice as an experimental model for cancer treatment, Physiol. Res. 65 (2016) S441–s453.

[58] M.S. Sasso, G. Lollo, M. Pitorre, S. Solito, L. Pinton, S. Valpione, G. Bastiat, S. Mandruzzato, V. Bronte, I. Marigo, J.P. Benoit, Low dose gemcitabine-loaded lipid nanocapsules target monocytic myeloid-derived suppressor cells and potentiate cancer immunotherapy, Biomaterials 96 (2016) 47–62.

[59] T. Wurdinger, K. Deumelandt, H.J. van der Vliet, P. Wesseling, T.D. de Gruijl, Mechanisms of intimate and long-distance cross-talk between glioma and myeloid cells: how to break a vicious cycle, Biochim. Biophys. Acta 1846 (2014) 560–575.

[60] A. Tuettenberg, K. Steinbrink, D. Schuppan, Myeloid cells as orchestrators of the tumor microenvironment: novel targets for nanoparticular cancer therapy, Nanomedicine (London, England) 11 (2016) 2735–2751.

[61] B. Raychaudhuri, P. Rayman, J. Ireland, J. Ko, B. Rini, E.C. Borden, J. Garcia, M.A. Vogelbaum, J. Finke, Myeloid-derived suppressor cell accumulation and function in patients with newly diagnosed glioblastoma, Neuro-Oncology 13 (2011) 591–599.

bioavailability, Biomaterials 31 (2010) 7542–7554.